University of Twente

EEMCS / Electrical Engineering
Control Engineering

Teleimpedance control of Unmanned Aerial Vehicles

W. (Wessel) Straatman

BSc Report

Committee:
Prof. dr. ir. S. Stramigioli
Dr. R. Carloni
A.Y. Mersha,MSc
Prof. dr. ir. A. de Boer

August 2012

Report nr. 023CE2012
Robotics and Mechatronics
EE-Math-CS
University of Twente
P.O. Box 217
7500 AE Enschede
The Netherlands

Teleimpedance control of Unmanned Aerial Vehicles

W. Straatman, A.Y. Mersha MSc, dr. R. Carloni

***Abstract*—For precise and accurate contact-related tasks of an Unmanned Aerial Vehicle (UAV), equipped with an end-effector, full control over motion and contact forces is desired. Teleimpedance control allows a human operator to send an impedance and motion profile to the end-effector, allowing full control over the contact-related task at hand.**

An estimation of the human arm impedance for the lower frequency range is determined by approximating the stiffness of the arm, and it is used to create a reference impedance for the end-effector of the vehicle. At the same time, the motion profile is used to control the motion of the end-effector.

A method for human arm impedance estimation has been designed which uses the MTi inertial sensor from Xsens. A method for force measurements has been designed that uses the Omega6 haptic interface. This method was verified through simulation and experiments. The idea of teleoperation of a human arm impedance approximation is validated through simulations with the programme 20Sim. Although experimental verification has been inconclusive due to measurement noise, simulations show promising results with regards to the teleimpedance control.

I. Introduction

More and more, researchers investigate the use of robotics for contact-related tasks like performing maintenance on power lines or inspection on higher ground, e.g. tall buildings or chimneys [1]. To perform contact-related tasks the UAV is equipped with an end-effector [2]. The end-effector can approach the environment with certain impedance, of which inertia, stiffness and damping can all be set through a controller. Currently, these tasks are often a costly, monetary as well as time-wise, and dangerous procedure. Big structures have to be built up to hold the weight of one or several person(s) and cranes might have to be deployed. The altitude, possible high voltages and similar hazards are reasons why inspection on higher ground can also be a dangerous task.

Being able to control both the motion profile that the end-effector follows, as well as the impedance, gives a human operator full control over the force at which the environment is approached. This allows precise contact-related tasks of the end-effector if a versatile reference for the motion and impedance is found. A requirement is that the human operator needs some kind of 'view' of the situation. This could be achieved through a feedback of the force working on the end-effector.

Human arm impedance can serve as a suitable reference value for the impedance control. Human arm impedance is a versatile characteristic, humans (often unknowingly) continuously change the impedance of the arm based on the situation or problem they encounter. It is also easy for a human to change the position of the arm.

A method for teleoperation of reference values to replicate the human arm impedance to a robot has been developed by Ajoudani et al [4]. They propose a measurement of electromyography (EMG) signals of the muscles to estimate arm impedance. EMG measurements, however, require a lot of precisely placed EMG sensors. Since the human operator of the UAV is someone skilled in the field of the task at hand for the UAV (e.g. inspection), and not in the field of EMG sensing, a different method for human arm impedance estimation is required.

The proposed method in this paper describes impedance estimation through force and inertial measurements during motion of the arm. Earlier work performed by Artemiadis et al [3] shows promising results for human arm estimation through force and inertial measurements.

It is proposed that, from human arm motion, force and inertial data is measured, impedance of the human arm is approximated through stiffness estimation, and replicated on the slave site. The human operator experiences a force feedback giving information on the force working on the end-effector, when in contact with unknown surroundings. Vibrotactile feedback will be used as force feedback. Previous research, e.g. by Cheng et al, has shown that humans are well capable of relating a certain vibrational pattern to an actual value of interest [5].

Goal of the work is to develop a feasible method to allow human arm motion and impedance to be used as reference for the UAV end-effector, through estimation of the impedance through inertial and force measurements. The impedance profile will be teleoperated to the end-effector and the human operator is provided with force feedback information on the force working on the end-effector. The proposed method should be validated in simulations and verified through experiments.

II. Analysis

A. Telemanipulation scheme

Fig. 1 displays the telemanipulation scheme. Through force, position and acceleration measurements, the stiffness characteristic of the human arm is estimated. Together with the position, which is used as a reference for the motion of the end-effector, this stiffness characteristic is used in the PD controller on the slave site. When in contact with a surrounding environment, the end-effector experiences a

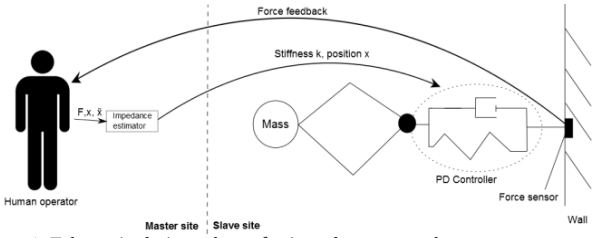

Figure 1. Telemanipulation scheme for impedance control.

force equal to but opposite in direction to the force it exerts on the surroundings. This force is measured and fed back to the human operator, who perceives this data through vibrotactile feedback. It is up to the human operator to decide whether or not to change the motion and/or impedance, based on this vibrotactile feedback.

B. Modelling

Master site

The human forearm is modelled as a rigid body with mass m, length L, diameter d, moment of inertia J and stiffness and damping parameters in both the rotational and translational domain. The centre of mass is assumed to be located in the centre of the body.

The lower part of the arm is modelled, from the elbow up and until the hand. The specifics of the human hand, like specific finger pose and shape, are not relevant for this application, therefore the human hand is simply modelled as a part of the rigid body.

The assumption made is that the upper arm can exert forces and torques in all directions to give the lower arm its desired position and/or orientation. Due to this assumption, the upper arm (and rest of the human body) can be represented by a set of forces and torques working on one part of the human arm.

It is reasonable to assume that there is both a damping factor and a stiffness factor, both rotational as well as translational. The damping factor represents for example friction, viscosity or air resistance, dependent on the configuration of the arm in real life [3]. The stiffness is the parameter that represents the flexing and tensing of the muscles, which causes a difference in arm impedance [3].

The rigid body has 6 degrees of freedom, being x, y, z, θ_x, θ_y, θ_z. Fig. 2 is a sketch of the human arm model. The position of the body is described by the x,y and z coordinates, and the rotation around the centre of mass is described by θ_x, θ_y, θ_z. The 6 degrees of freedom can be controlled independently, however, a change in rotation around the centre of mass also changes the position of the end in x, y, z coordinates.

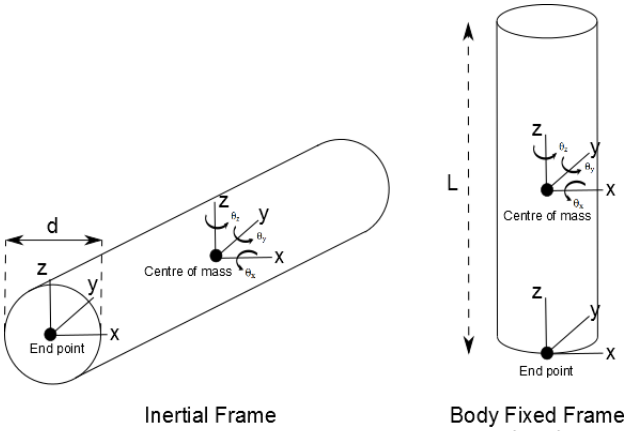

Figure 2. 6DOF human arm model represented in both a body fixed frame as well as inertial frame.

In the case that it is demanded that the end point does not move, a reaction force equal in size but in opposite direction is needed to keep the end point position constant. This reaction force results in a reaction torque in the centre of mass, equal to the magnitude of the reaction force times the length of the arm L/2. This is graphically displayed in fig. 3.

The velocities are represented in two frames, a body fixed frame, rotating along with the body, and an inertial frame, where Newton's laws apply.This prevents having to take fictitious forces into account in the rotating reference frame.

The modelling is done using a bond graph approach [6]. Bond graphs are used because they can easily represent the dynamic relations between several different domains, e.g. the translational and rotational domain. The bond graph model can be found in fig. 4.

The RTF elements contain the 3D rotation matrix, which is build up through the individual rotation matrices for x, y and z [7].

$$R_x = \begin{bmatrix} 1 & 0 & 0 \\ 0 & \cos\theta_x & -\sin\theta_x \\ 0 & \sin\theta_x & \cos\theta_x \end{bmatrix}, R_y = \begin{bmatrix} \cos\theta_y & 0 & \sin\theta_y \\ 0 & 1 & 0 \\ -\sin\theta_y & 0 & \cos\theta_y \end{bmatrix},$$

$$R_z = \begin{bmatrix} \cos\theta_z & -\sin\theta_z & 0 \\ \sin\theta_z & \cos\theta_z & 0 \\ 0 & 0 & 1 \end{bmatrix}$$

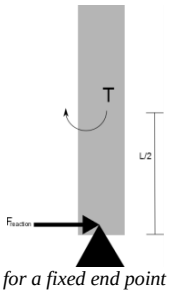

Figure 3. Reaction force for a fixed end point demand in rotating scenario.

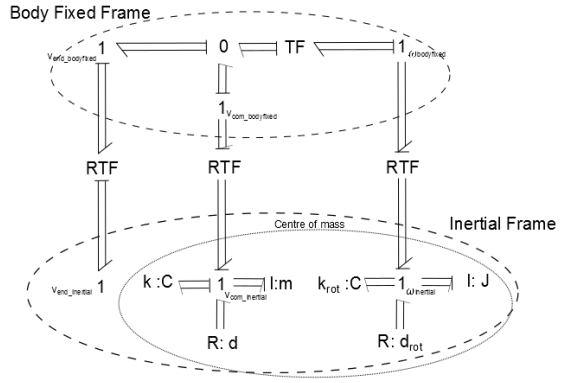

Figure 4. Bond graph model of the human arm.

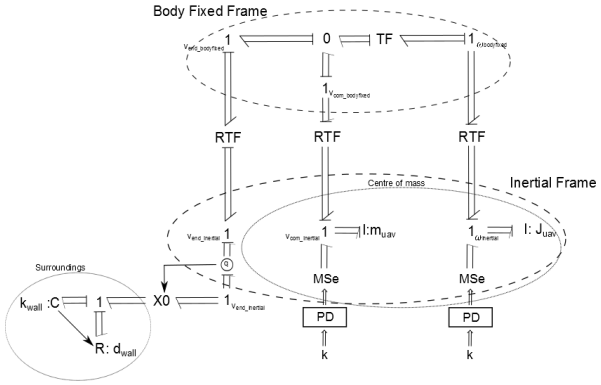

Figure 5. Bond graph model of end-effector interaction with solid wall.

A matrix multiplication RxRyRz gives the desired 3d rotation matrix.

$$R_{xyz} = \begin{bmatrix} \cos\theta_y \cos\theta_z & -\cos\theta_y \sin\theta_z & \sin\theta_y \\ \cos\theta_x \sin\theta_z + \sin\theta_x \sin\theta_y \cos\theta_z & \cos\theta_x \cos\theta_z - \sin\theta_x \sin\theta_y \sin\theta_z & -\sin\theta_x \cos\theta_y \\ \sin\theta_x \sin\theta_z - \cos\theta_x \sin\theta_y \cos\theta_z & \sin\theta_x \cos\theta_z + \cos\theta_x \sin\theta_y \sin\theta_z & \cos\theta_x \cos\theta_y \end{bmatrix}$$

This rotation matrix corresponds to a right handed rotation of x, y and z.

The transformer element gives the contribution in the translation of the end point of the arm due to rotation. This can be represented through the following matrix [8]. The position vector is the body fixed frame end point position.

$$\begin{bmatrix} 0 & z_p & -y_p \\ -z_p & 0 & x_p \\ y_p & -x_p & 0 \end{bmatrix}, \text{where } \begin{bmatrix} x_p \\ y_p \\ z_p \end{bmatrix} = \begin{bmatrix} 0 \\ 0 \\ L/2 \end{bmatrix}.$$

The dynamic equations can be derived from the bond graph and are given in (1a) and (1b).

$$0 = m\ddot{x}_{com}(t) + d\dot{x}_{com}(t) + kx_{com}(t) \quad (1a)$$
$$0 = J\ddot{\theta}(t) + d_{rot}\dot{\theta}(t) + k_{rot}\theta(t) \quad (1b)$$

Slave site

The end-effector is also modelled as a rigid body with 6 degrees of freedom. It has mass m, length L, diameter d and moment of inertia J. A PD controller , which is essentially a spring-damper relation, ensures that motion of the end-effector takes place for certain reference position and at certain impedance. The model can be found in fig. 5.

Opposed to the human arm, which was assumed to be able to move without any spatial limitations (e.g. a wall or a robust object), the end-effector is limited in its movement due to the (to be inspected) surroundings. These surroundings are taken into account for the slave site. The surrounding is modelled through a spring-damper combination with high stiffness and damping values, ensuring a zero velocity on impact with the surrounding.

To represent the relation between the 'compression' of the wall and the damping force, the damper is modelled using the Hunt-Crossley method, which utilises the non-linear relation $F_d(t) = \lambda\dot{x}(t)x(t)$ where λ is a damping coefficient [9]. Since for more compliant surroundings the Hunt-Crossley model gives better results, it is also more suitable to use in case of unknown surroundings [9].

The contact between surrounding and end-effector end point is modelled through an X0 switching element. The X0 ensures that the end point 1-junction is only connected to the RC-junction if the end point is at (or past) a certain position, the position of the surroundings in the inertial frame. A more detailed explanation can be found in appendix A.

The dynamic equations can be derived from the bond graph. The force and torque from the PD controllers are represented by their proportional and differential gains P and D. The difference between the reference position and angle obtained from the human arm and the actual position and angle of the end-effector give the error of the controller. The equations are given in (2a) and (2b).

$$0 = m\ddot{x}_{com}(t) + D(\dot{x}_{arm}(t) - \dot{x}_{com}(t)) + P(x_{arm}(t) - x_{com}(t) \quad (2a)$$
$$0 = J\ddot{\theta}(t) + D_{rot}(\dot{\theta}_{arm}(t) - \dot{\theta}(t)) + P_{rot}((\theta_{arm}(t) - \theta(t)) \quad (2b)$$

C. Human arm impedance estimation

The equations of motion for a the human arm model follow as (3a), for translations, and (3b), for rotations around the centre of mass [10].

$$F(t) = m\ddot{x}(t) + d\dot{x}(t) + kx(t) \quad (3a)$$
$$T(t) + \frac{L}{2} * F(t) = J\ddot{\theta}(t) + d_{rot}\dot{\theta}(t) + k_{rot}\theta(t) \quad (3b)$$

From the equations of motion, it is possible to derive an expression for k. When it is assumed that the damping is low and we work around low velocities the damping force can be neglected. This does, however, not imply we can also neglect the force containing the acceleration, $m\ddot{x}(t)$, because the mass is usually much greater than the damping coefficient, and, even though we work around low velocities, a rapid change in small velocities still results in a high acceleration. The low velocity assumption demands the operating condition under which the movement takes place. It also removes the damping force from the equations of motion.

The expression for k that follows is $\frac{F(t)-m\ddot{x}(t)}{x(t)} = k$. The mass m is assumed to be known because it can be measured, therefore when there are measurements of F(t), x(t) and $\ddot{x}(t)$ it is possible to approximate k. Similar reasoning holds for the rotational case.

The estimated stiffness from the human arm is sent as a reference value to the end-effector. It is demanded that the impedance profile at the end-effector is similar to the estimated impedance profile of the human arm. The resonant frequency ω_0, equal to $\sqrt{\frac{k}{m}}$, is required to be the same, but the mass of the human arm and the mass of the end-effector are not necessarily equal. Therefore, stiffness is scaled by the mass ratio to ensure equal resonant frequency characteristics.

D. Simulations

A simulation of the telemanipulation loop process has been performed using 20Sim. The human operator's arm (m=1 kg) provides a reference motion of x=0.1 m, with a stiffness of 300 N/m. The end-effector (m=0.2 kg) attempts to move to x=0.1 m as well, at the estimated impedance profile. The impedance profile is approximated through a stiffness estimation of the human arm, which is scaled by the mass ratio. The end-effector encounters a solid wall at x=0.09 m, so cannot move beyond this point, and as a result experiences a force. This force is fed back through vibrotactile feedback to the human operator. The vibrotactile feedback has amplitude and frequency changing linearly when the force on the end-effector changes.

At t=20 s the human operator makes a decision to lower the impedance. This results in a lower force working on the end effector, and a change in both amplitude and frequency of the vibrotactile feedback that the human experiences.

The position of the arm and end-effector is found in fig. 6a, the stiffness values in fig. 6b, the force working on the end-effector in fig. 6c and the vibrotactile feedback in fig. 6d. The spikes in the estimated stiffness are caused by small errors in differentiation of the velocity, representing (indirect) acceleration measurements. In real measurements this does not occur because direct measurement of the acceleration is used in the actual setup.

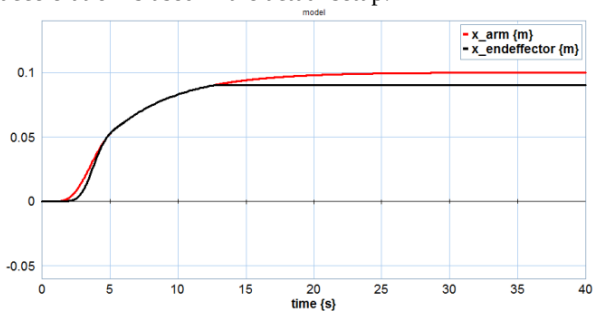

Figure 6a. Position of human arm and tracked motion of end-effector.

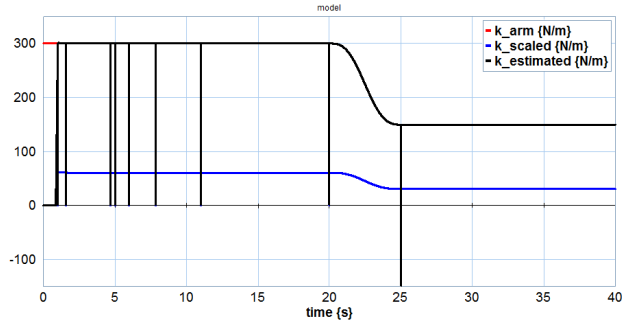

Figure 6b. Stiffness value of human arm, estimated stiffness value after force and inertial measurements and stiffness value scaled by mass ratio.

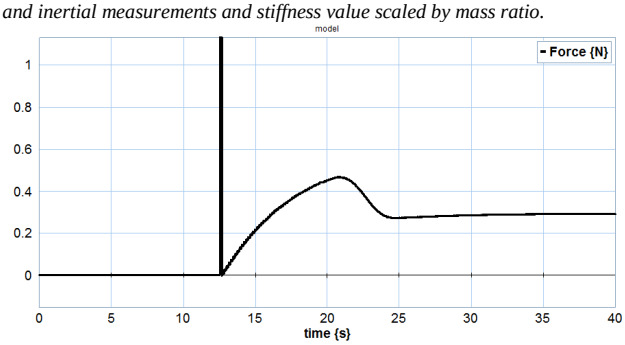

Figure 6c. Force working on the end-effector during contact with solid wall.

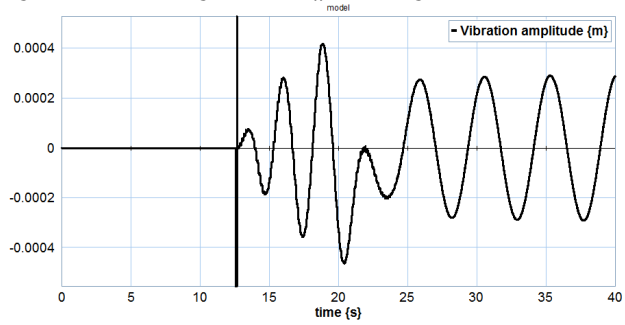

Figure 6d. Vibrotactile force feedback to human operator.

III. REALISATION

A. *Experimental set-up*

Earlier derivations have shown that for reliable stiffness approximation measurements of the force, the acceleration and the position are required. Also, the human operator should be able to perceive information on the UAV surroundings through force feedback. Force measurements and inertial measurements are available, position will be estimated from the inertial measurements.

Force measurement

To get a reliable impedance estimation, an accurate force measurement is required whilst not influencing the actual motion of the arm. The human operator will use the Omega6 haptic interface with admittance display mode for this purpose. Admittance display measures force and displays displacement, opposed to impedance display which measures displacement and displays force [11][12].

The admittance mode will equip PD control on the position. By changing the position of the haptic interface equipped with a force/torque sensor, the force exerted by the operator can be measured, since it is equal to but opposite in direction of the measured force. An advantage of this set up is that it is less prone to small errors or perturbations in movements that are unintentional, since the haptic interface will only move when a certain force is applied [12]. Through simulations, several values for P and D are investigated. Simulations show that suitable values are P=1 and D=0.5. The simulations can be found in appendix B.

Inertial measurements

The Xsens MTi inertial motion sensor will be used to measure the acceleration of the human arm movement [13]. The Xsens communicates through the RS232 protocol and measures inertial data and magnetic field data [14].

The displacement follows from double integration of the acceleration signal. Because of integration drift due to noise arising in the acceleration measurements, a filter was placed in between measurement and integration.

To read out measurement results, Matlab and Simulink are used. A description of the Matlab .m files communicating with the Xsens can be found in appendix C. These .m files are adaptations of code written by Technische Universität München, obtained through Xsens. The Simulink model has to run real time, a description of its code can be found in appendix D.

Vibrotactile force feedback

MOT-10 closed pager vibration motors will be used as a means of feedback mechanism for the human operator. The MOT-10 motors have amplitude and frequency coupled which can be controlled through varying the voltage. Relating the force feedback to a reference voltage creates a scale from which the human operator can sense whether or not the force on the end-effector is becoming too much. A simple linear scale varying from 0 N to 20 N (the maximum the end-effector can have without damaging) is chosen, and can be found in fig. 7.

Based on the perceived force and surroundings, the human operator can decide to change the approach towards the surroundings, or change the impedance of the end-effector by changing arm impedance.

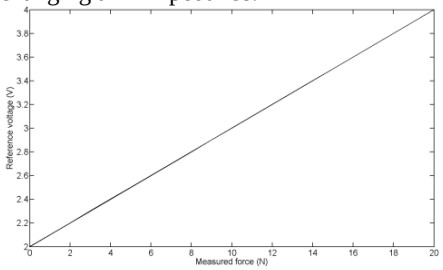

Figure 7. Reference scale for vibrotactile motors.

B. *Experimental results*

Force measurements

Using the Omega6 haptic interface, the proposed method for force measurement of the human arm is verified. Three situations were analysed:
- Force measurement for P=1, D=10, arm moving to x=0.02 m and back.
- Force measurement for P=1, D=0.5, arm moving to x=0.02 m and back.
- Force measurement for P=1, D=0.1, arm moving to x=0.02 m and back.

The first scenario, where D=10 so a low damping is applied, gave stability issues. The haptic interface started to oscillate and was not able to track motion and accurately provide a force measurement. The cause is the low value for the damping. The simulations in appendix B showed that for this configuration the device would start oscillating, and this was verified in the experiments.

The second scenario, where D=0.05, is the scenario that is, according to simulations, the most suited for reliable force measurements. Fig. 8a gives the imposed position input. Fig. 8b gives the force measurement. The force measurement responds fast. The motion is not perceivably hindered by the damping force applied by the controller.The last scenario, where D=0.01, is expected to display a more direct force measurement. Fig. 9a gives the imposed position input. Fig. 9b gives the force measurement. The force measurement indeed responds really fast, but therefore is also sensitive to really small disturbances like vibrations of the human arm. Also, when comparing figs. 8b and 9b, one immediately notes the higher force required for D=0.01. This is intuitively correct due to a higher damping force working against the motion, and implies a less reliable motion tracking.

The position PD controller setup with P=1 and D=0.5 therefore is shown to give most reliable force measurement results. Simulations already indicated this, and experiments have verified this conclusion.

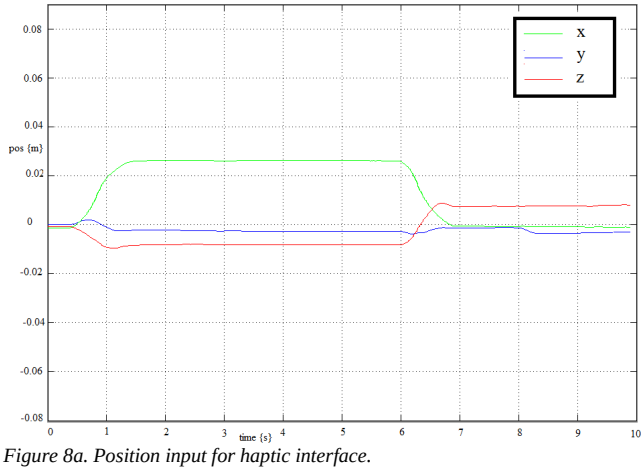

Figure 8a. Position input for haptic interface.

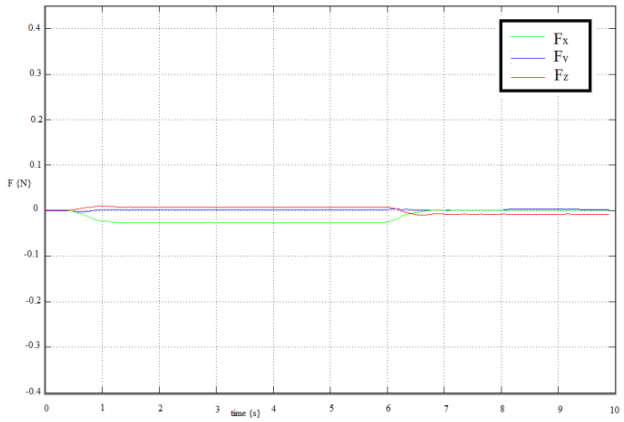

Figure 8b. Force measurement from haptic interface for P=1 and D=0.5.

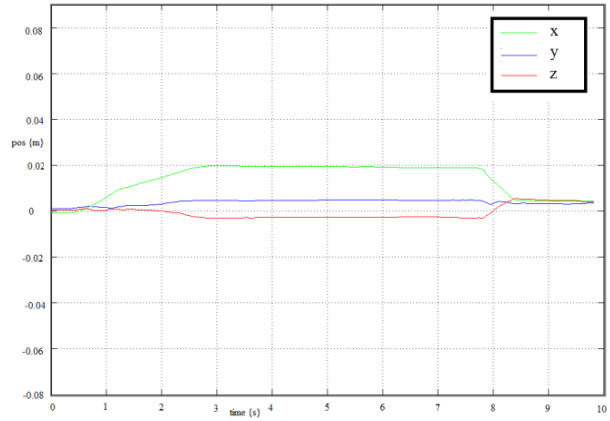

Figure 9a. Position input for haptic interface.

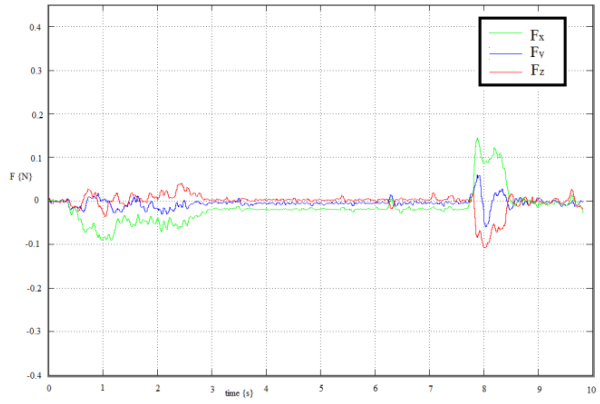

Figure 9b. Force measurement from haptic interface for P=1 and D=0.1.

Inertial measurements

Using Simulink, a realtime measurement of the Xsens MTi inertial data is performed. The acceleration in x, y and z direction is measured and integrated twice to get a position approximation. Fig. 10 displays acceleration measurements from t=10s to t=14s, when the Xsens sensor is not moving. A constant value correction has been done to eliminate the gravity component. The measurements have been initiated about 20 minutes after connecting the Xsens so that it could 'warm up' as suggested by the Xsens support website [13].

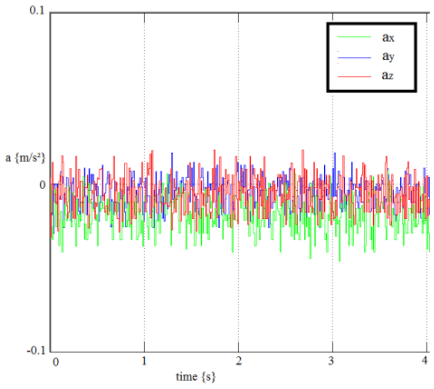

Figure 10. Acceleration measurements for non-moving Xsens motion sensor.

As can be seen, there is presence of noise in the acceleration measurements. Frequency analysis, which can be found in appendix E, shows that most noise arises from about 6 Hz and on. Based on this spectrum, a suitable filter can be designed to filter out the noise.

Choice is made for a higher order Chebyshev filter, due to its characteristic of steep rolloff slope [15]. The choice is made to insert an 8th order lowpass filter with a cutoff frequency at 2Hz.

The filter is implemented in the measurement set up. Fig. 11 describes the acceleration measurement after filtering, and shows a clear periodic noise component around a certain offset.

Since the offset is not a constant offset, and there is also still low frequent noise present, the position estimation is expected to still show an integration drift. The calculated position estimation is shown in fig. 12. For a non-moving inertial sensor, the position offset is already around 5 metres after 5 seconds of measurements have passed. As appendix E shows, this gives unreliable results for the stiffness estimate.

Use of the Xsens MTi sensor for impedance approximation

The performed measurements show that the Xsens MTi, in its current set up, is not suitable for human arm impedance estimation due to a significant drift in position estimation. The Xsens is suitable for acceleration measurements, but a working impedance estimation set up will require a more accurate position measurement as well.

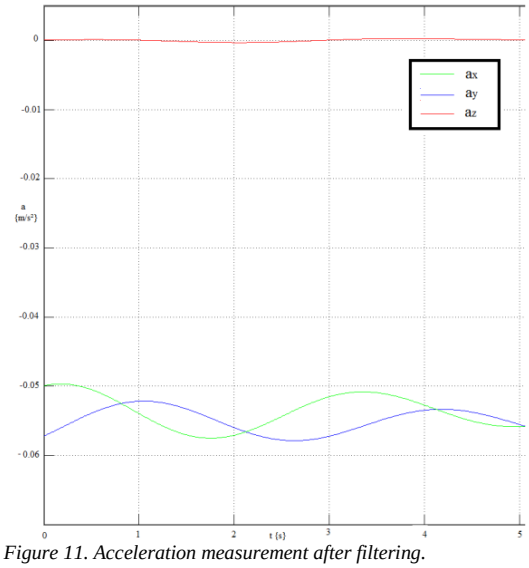

Figure 11. Acceleration measurement after filtering.

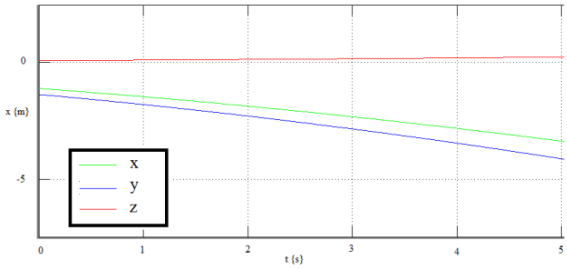

Figure 12. Position estimation after filtering, for a non-moving inertial sensor.

IV. Conclusions and Recommendations

A method has been designed that allows use of an impedance profile, estimated from the movement of a human arm, as a reference for the equipped end-effector of an Unmanned Aerial Vehicle, used for inspection and other contact-related tasks of unknown surroundings and objects located at altitude.

A bond graph model of the human arm and the end-effector has been made in the simulation programme 20Sim. Simulations have been done to verify the feasibility of the proposed design. The results of these simulations show promising results.

Force measurements have been performed using the Omega6 haptic interface. Both simulation and experimental validation have shown that a position PD controller setup where P=1 and D=0.5 provides most reliable force measurements.

The Xsens MTi inertial measurement sensor has been used for experimental verification of the designed method. Present noise in acceleration measurements has inadequately been removed by filtering. The frequency spectrum of the noise has been investigated and a proper filter has been designed, though the position estimation through double integration of the noisy filtered signal still shows a lot of integration drift, making the measurements unsuitable for actual human arm impedance approximation.

For future work, it is advised to continue to look into the application because simulations show promising results. Looking into more advanced ways of filtering the Xsens measurement noise, based on the noise data gathered in this work, is an option.

When this does not succeed a different recommendation is to work with a separate position sensing device together with a device capable of doing inertial measurements. For outdoor applications one could consider a motion sensor equipped with a GPS and a Kalman filter, like the Xsens MTi-G. For indoor applications, however, it is advised to use position sensing based on optical or magnetic characteristics, combining it with an accelerometer (like the Xsens MTi used in these experiments). Trying to estimate position based on double integration of acceleration measurements should be prevented because of the inaccuracies it provides in impedance approximation.

Together with the proposed force feedback, the human operator can easily operate the UAV end-effector using arm motion. A possible application is the mapping of human arm motion to an approach motion of the end-effector, enabling the approximated impedance of the arm as the actual impedance of the end-effector. Through interpretation of the vibrational force feedback, the operator has a conceptual view on the surroundings of the end-effector and can work on performing his or her task without risking damaging the end-effector.

Appendix A: X0 junction

The XO-junction is an adapted 0 junction that acts like a switch between contact and non-contact mode between two junctions. In this case, the X0 switches between contact and non-contact between the end-effector and a (solid) unknown surrounding. The X0 switches based on a reference signal, being the position of the end-effector end point. When the position is at or beyond the position of the surroundings, the bonds are connected. Otherwise, no connection is there so the end-effector does not perceive any influence from surroundings.

The port connected to the wall has fixed flow out causality. This means that it has a fixed effort in causality, which makes sense because this effort, working on the end-effector end point, is the force the end-effector endures when in contact.

The code for the X0 junction is given below.

```
variables
  boolean hidden ev;
  real x;
```

```
  real wall;
  real zero[3,1];

equations
  wall = 0.1; //wall location
  x = pos[1,1];
  zero = [0;0;0];
  ev = event(x);
  p1.e = if (x>=wall) then p2.e else zero end;
  p2.f = if (x>=wall) then p1.f else zero end;
    F = p1.e; //force working on end-effector end
point
```

APPENDIX B: FORCE MEASUREMENT PD CONTROL DESIGN

A proportional gain increase improves tracking of the motion but can cause an overshoot, a differential gain opposes the overshoot but also improves (decreases) settling time [6]. It is expected that when D gets too large, it will take the set up much longer to 'settle' into its configuration, so the force measurement accuracy will be less until after a certain amount of time. Therefore, a correct balance will have to be found between the ability to follow human arm movement without influencing it, and accurate force measurement.

It is important to notice the trade-off between the two. The optimal trade-off is found through simulation of several different values for P and D. Fig. B1a and B1b show force measurement and position tracking for low D of 0.1 and proportional gain of 1. The motion being tracked is a movement of the arm from x=0m to x=2m.

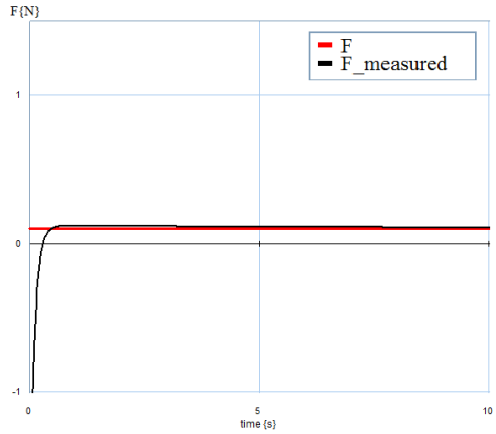

Figure B1a. Force measurement for P=1 and D=0.1.

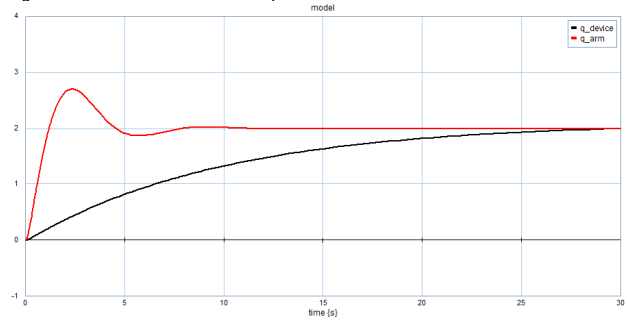

Figure B1b. Motion tracking, for P=1 and D=0.1.

The force is accurately measured, but tracking the motion profile takes time. Therefore, differential gain is increased to 10. Fig. B2a and B2b give force measurement and motion tracking for P=1 and D=10.

The oscillation implies that D is now too high, because D is inversely proportional to a damping and higher damping damps out the oscillations. The ideal value for D will therefore lie in between 0.1 and 10. A value of D=0.5 is simulated for P=1. The force measurement and motion tracking is given in figs. B3a and B3b.

Within reasonable time, both the force measurement is accurate and the position of the controller is almost equal. This configuration therefore satisfies the aforementioned requirements and gives a reliable force measurement.

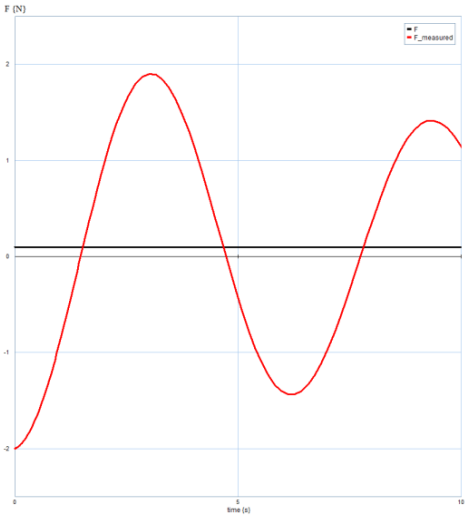

Figure B2a. Force measurement for P=1 and D=0.1

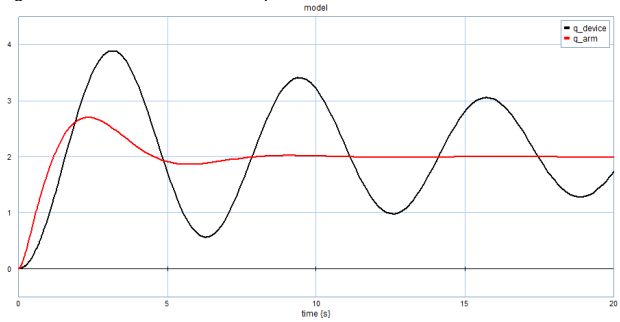

Figure B2b. Motion tracking, for P=1 and D=10.

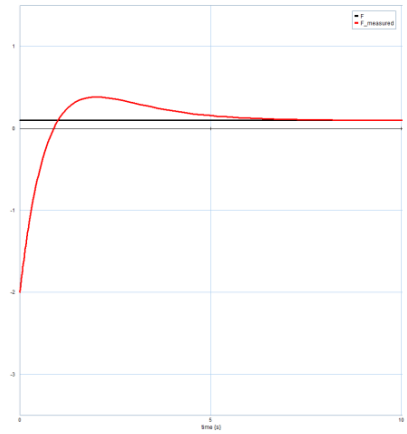

Figure B3a. Force measurement for P=1 and D=0.5.

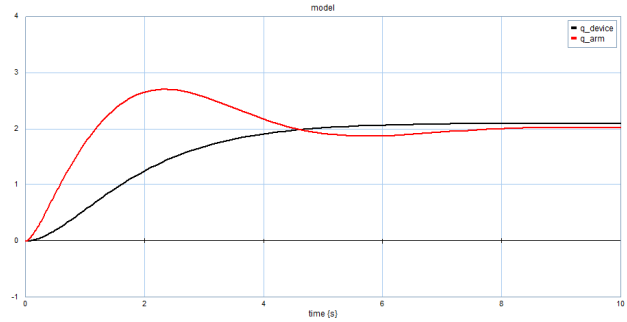

Figure B3b.Motion tracking, for P=1 and D=0.5.

APPENDIX C: MATLAB CODE

Callback_Simulink_MT_Start.m

The Callback_Simulink_MT_Start.m file initiates the Xsens motion tracker communication. Users can change optional parameters like sample frequency and the COM-port where the device is attached to. Running this file instantiates an object handle containing the motion tracker in measurement mode.

Simulink_MT_get_data.m

The Simulink_MT_get_data file retrieves inertial data from the properly initialised motion tracker. It obtains acceleration, angular velocity, magnetic field magnitude and Euler angle data.

Callback_Simulink_MT_stop.m

The Callback_Simulink_MT_stop file does nothing more and nothing less than properly shutting down the motion tracker and clearing the handle.

APPENDIX D: SIMULINK REAL TIME MEASUREMENTS

The Soft Real Time block runs C-code compiled as a MEX-file. It is necessary that the MEX-compilation is done correctly, a MEX32 file does not work on a 64-bit MATLAB version. A C-compiler might be required, use the command ‘ mex –setup ‘ in the MATLAB workspace to see MATLAB’s compiler suggestions. For this work, Microsoft Windows SDK 7.1 was used [16]. The code for the real time measurements was obtained from the Mathworks Matlab Central file exchange [17].

APPENDIX E: ANALYSIS OF NOISY SIGNAL

An average of the noise signal was calculated, using Matlab, by taking 100 measurements and taking the average. This is repeated N times to produce fig. E1, displaying the average of the noise of the acceleration, in y direction for N=100.

As fig. E1 shows, the mean value of the noise is not constant, nor is it equal to zero.

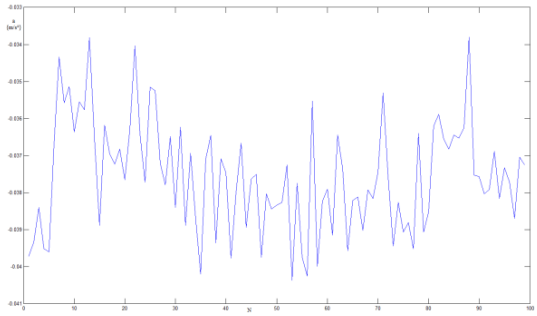

Figure E1. Average noise of acceleration in y direction.

In order to investigate the frequency behaviour of the noise a spectrum measurement of the noise has been made.

Data was sampled at 100Hz and Matlab’s Fast Fourier Transform function was used to create the spectrum. The spectrum can be found in fig. E2.

The choice is made to insert an 8th order lowpass Chebyshev filter with a cutoff frequency at 2Hz. The transfer function of the filter is plotted in fig. E3.

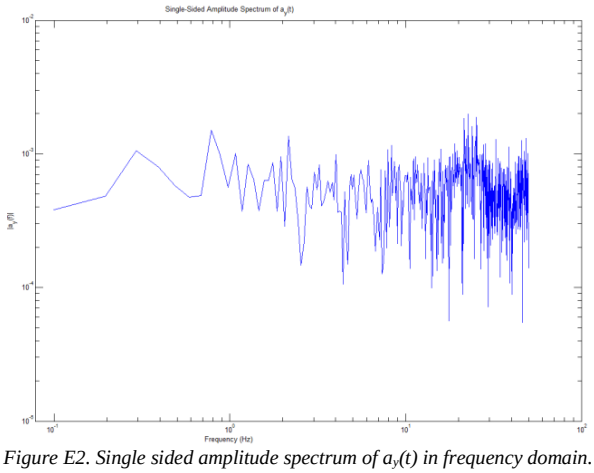

Figure E2. Single sided amplitude spectrum of $a_y(t)$ in frequency domain.

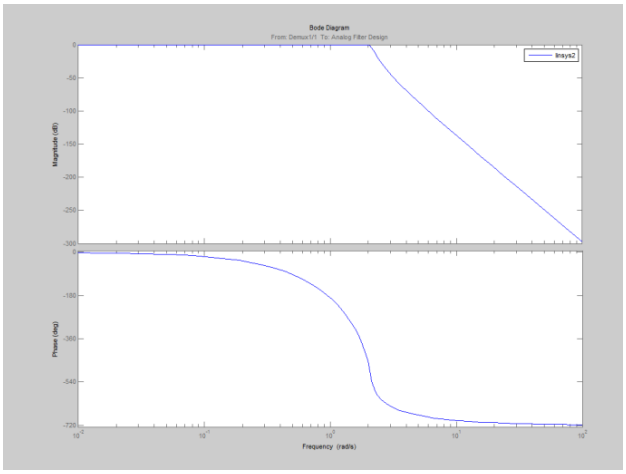

Figure E3. Bode plot of 8th order Chebyshev low pass filter with cut-off frequency of 2Hz.

To look at the influence of the noisy measurements on impedance estimation, a noisy signal, through a random generator with comparable amplitude to the measured noise signal, located around the average as measured earlier, is used in simulation to approximate stiffness of the human arm. Fig. E4 shows the approximated stiffness for k=100 N/m during movement of the arm over 1 metre from t=1s to t=6s.

The estimated stiffness does not come anywhere near the actual stiffness, using this approximation as reference for the actual end-effector will provide a lot of issues.

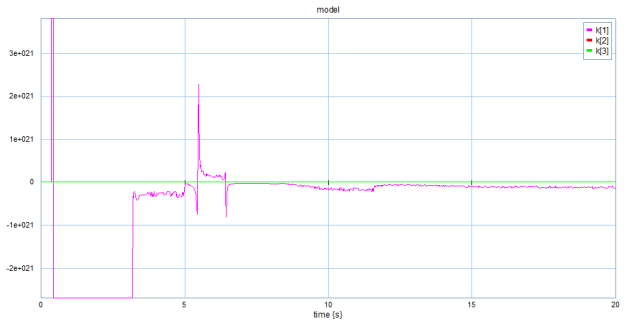

Figure E4. Stiffness approximation for noisy signal, with k=100 N/m.

REFERENCES

[1] Airobots project [online], http://www.airobots.eu

[2] M. Fumagalli, R.Naldi, R. Carloni, A.Q.L. Keemink, F. Forte, A. Macchelli, S. Stramigioli and L. Marconi, "Quadrotor Interacting with a Remote Environment: Control of a Flying Hand", 2012

[3] Panagiotis K. Artemiadis, Pantelis T. Katsiaris, Minas V. Liarokapis, and Kostas J. Kyriakopoulos, "Human Arm Impedance: Characterization and Modeling in 3D Space", *IEEE/RSJ International Conference on Intelligent Robots and Systems (IROS)*, 2010

[4] A. Ajoudani, N. G. Tsagarakis and A. Bicchi, "Tele-Impedance: Towards Transferring Human Impedance Regulation Skills to Robots", *IEEE International Conference on Robotics and Automation*, 2012

[5] Andrew Cheng, Kirk A. Nichols, Heidi M. Weeks, Netta Gurari, and Allison M. Okamura, "Conveying the Configuration of a Virtual Human Hand Using Vibrotactile Feedback", *IEEE Haptics Symposium*, 2012

[6] P.C. Breedveld, "Integrated Modeling of Physical Systems - Dynamic Systems part 1 thru 3", *Open university*

[7] K.F. Riley, M.P. Hobson, S.J. Bence, "Mathematical Methods for Physics and Engineering", *Cambridge*

[8] P.C. Breedveld, "3D Kinematics Notation", *University of Twente*, 2008

[9] Nicola Diolaiti, Claudio Melchiorri, Stefano Stramigioli, "Contact Impedance Estimation for Robotic Systems", *IEEE Transactions on robotics*, vol. 21, no. 5, October 2005

[10] Paul M. Fishbane, Stephen Gasiorowicz, and Steve Thornton, "Physics for Scientists and Engineers", third edition, *Pearson Education*

[11] Martin Wassink, "Design and Implementation of a Haptic Display Environment for the Fokker Flight Stick", Individual Design Assignment, *University of Twente*, 2005

[12] W Manikantan Nambi, William R. Provancher and Jake J. Abbott, "On the Ability of Humans to Apply Controlled Forces to Admittance-Type Devices", *Advanced Robotics 25*, 2011.

[13] Xsens: 3D motion tracking [online], http://www.xsens.com

[14] Xsens, "MTi and MTx User Manual and Technical Documentation"

[15] Alan S. Morris, Reza Langari, "Measurement and Instrumentation: Theory and Application", *Butterworth-Heinemann*

[16] Microsoft Windows SDK 7.1 for Windows 7 [online], http://www.microsoft.com/en-us/download/details.aspx?id=8279

[17] Mathworks Matlab Central [online], http://www.mathworks.com/matlabcentral